Journal of Electrotechnology, Electrical Engineering and Management (2025)
Clausius Scientific Press, Canada
DOI: 10.23977/jeeem.2025.080107
ISSN 2560-6697 Vol. 8 Num. 1

Sensorless Control of PMSM Based on an Improved Super-Twisting Sliding Mode Observer

Baihui Chen[1,a], Fengxiang Chen[1,b,*]

[1]College of Automotive Studies, Tongji University, Shanghai, 201804, China
[a]2233489@tongji.edu.cn, [b] fxchen@tongji.edu.cn
**Corresponding author*

Keywords: Permanent Magnet Synchronous Motor, Sensorless control, Super-twisting sliding mode observer, Quadrature phase-locked loop

Abstract: This paper presents an enhanced fast super-twisting algorithm sliding mode observer for sensorless control of permanent magnet synchronous motors. The proposed method improves upon conventional super-twisting algorithms by incorporating a linear correction term, which simultaneously boosts convergence speed and reduces chattering effects. These enhancements lead to superior dynamic response and steady-state estimation accuracy. Stability is guaranteed through rigorous Lyapunov analysis, with explicit convergence conditions mathematically derived. For practical implementation, rotor position and speed are accurately extracted from the estimated extended back-EMF using an optimized signal processing chain combining low-pass filtering and quadrature phase-locked loop techniques. Comprehensive simulation studies validate the proposed observer's performance advantages over traditional super-twisting approaches, demonstrating significant improvements in both position and speed estimation accuracy. The results confirm the method's effectiveness and practical viability for high-performance sensorless PMSM drives.

1. Introduction

Permanent Magnet Synchronous Motor (PMSM) have become increasingly prevalent in industrial automation, new energy vehicles, household appliances, and aerospace applications owing to their superior efficiency, high power density, compact structure, and low maintenance requirements[1]. The growing adoption of PMSM across these diverse fields has created an urgent need for enhanced control precision and reliability. High-performance PMSM control critically depends on accurate rotor position information, traditionally obtained through mechanical position sensors. However, these sensors not only increase system cost and size but also compromise reliability and lifespan in harsh operating environments characterized by high temperatures, pressures, and vibrations[2]. Consequently, the development of advanced sensorless control techniques has emerged as a crucial research direction in PMSM control[3]. Current sensorless control strategies primarily fall into two categories: high-frequency signal injection methods and model-based approaches[4,5]. While high-frequency injection methods, which exploit PMSM saliency by injecting high-frequency voltages and extracting position information from current

responses, perform well at low speeds, they become ineffective at medium-high speeds due to spectral overlap between the injected signal and fundamental excitation. This limitation necessitates the use of model-based approaches for medium-high speed operation.

Various model-based techniques have been developed, including Model Reference Adaptive Systems (MRAS), Extended Kalman Filters (EKF), and Sliding Mode Observers (SMO). Po-ngam et al.[6] proposed an improved MRAS observer with proven stability conditions and enhanced dynamic characteristics through feedback gain design. However, MRAS methods remain highly sensitive to parameter variations[7,8], potentially leading to convergence issues when parameters deviate significantly from their nominal values. Quang et al.[9] developed a reduced-order parallel EKF structure that improved computational efficiency while maintaining estimation accuracy. Nevertheless, EKF's inherent computational complexity, involving extensive matrix and floating-point operations, imposes substantial processor requirements, limiting its practical applications.

Among these alternatives, SMO has gained prominence for medium-high speed sensorless control due to its structural simplicity, robustness, and ease of implementation[10]. However, conventional SMO suffer from significant chattering caused by switching functions in the control law. Researchers have proposed various improvements, including continuous function replacements for switching terms. The Super-Twisting Algorithm (STA) developed by Davila and Levant[11] effectively reduces chattering by embedding discontinuous functions in the first derivative of control inputs while maintaining convergence and robustness. Gonzalez and Evangelista[12,13] further enhanced this approach through adaptive-gain STA methods that improve estimation accuracy across wide speed ranges.

Despite these advances, higher-order sliding mode controllers still face limitations including slow convergence, delayed response to sudden disturbances, and residual high-frequency chattering near sliding surfaces. To address these challenges, this paper presents a novel Fast Super-Twisting Algorithm (FSTA) that incorporates a linear correction term to optimize the reaching law, enabling exponential state convergence and significantly improved dynamic performance. The proposed FSTA demonstrates enhanced responsiveness to input variations and external disturbances while maintaining smooth transitions near sliding surfaces, thereby further reducing chattering. Building on this algorithm, we develop a Fast Super-Twisting Sliding Mode Observer (FSTA-SMO) with rigorously derived stability conditions via Lyapunov theory. Rotor position and speed information are accurately extracted from extended back-EMF using a combined low-pass filter (LPF) and quadrature phase-locked loop (QPLL) approach. Comprehensive simulation results validate the FSTA-SMO's superior dynamic performance and steady-state accuracy, confirming its effectiveness for sensorless control applications.

2. Mathematical Model of Permanent Magnet Synchronous Motor

The voltage equations of the PMSM in the two-phase stationary reference frame can be expressed as:

$$\begin{bmatrix} u_\alpha \\ u_\beta \end{bmatrix} = \begin{bmatrix} R_s + pL_d & \omega_e(L_d - L_q) \\ -\omega_e(L_d - L_q) & R_s + pL_d \end{bmatrix} \begin{bmatrix} i_\alpha \\ i_\beta \end{bmatrix} + \begin{bmatrix} \lambda_\alpha \\ \lambda_\beta \end{bmatrix} \tag{1}$$

where, u_α, u_β denote the stator voltage, while i_α and i_β denote the stator currents. R_s is the stator resistance, and L_d and L_q are the stator inductances. The electrical angular velocity is given by ω_e , with p representing the differential operator. The back-EMF λ_α and λ_β can be expressed as:

$$\begin{bmatrix}\lambda_\alpha\\ \lambda_\beta\end{bmatrix}=\left[(L_q-L_d)(pi_q-\omega_e i_d)+\omega_e\varphi_f\right]\begin{bmatrix}-\sin\theta_e\\ \cos\theta_e\end{bmatrix} \tag{2}$$

where, φ_f represents the rotor flux linkage and θ_e denotes the electrical angle.

By combining Equations (1) and (2), the voltage equations can be reformulated to obtain the stator current differential equations:

$$\frac{d}{dt}\begin{bmatrix}i_\alpha\\ i_\beta\end{bmatrix}=\frac{1}{L_d}\begin{bmatrix}-R_s & -\omega_e(L_d-L_q)\\ \omega_e(L_d-L_q) & -R_s\end{bmatrix}\begin{bmatrix}i_\alpha\\ i_\beta\end{bmatrix}+\frac{1}{L_d}\begin{bmatrix}u_\alpha-\lambda_\alpha\\ u_\beta-\lambda_\beta\end{bmatrix} \tag{3}$$

3. Design of Conventional Super-Twisting Sliding Mode Observer

Compared with conventional sliding mode approaches, the Super-Twisting Algorithm-based Sliding Mode Observer (STA-SMO) effectively attenuates chattering by embedding the switching function within an integral term. When applying the STA to state observer design, the general mathematical representation takes the following form:

$$\begin{cases}\dfrac{d\hat{x}_1}{dt}=-k_1\left|\hat{x}_1-x_1\right|^{1/2}sgn(\hat{x}_1-x_1)+x_2+\rho_1(\hat{x}_1,t)\\ \dfrac{d\hat{x}_2}{dt}=-k_2 sgn(\hat{x}_1-x_1)+\rho_2(\hat{x}_1,t)\end{cases} \tag{4}$$

where, x_1 and x_2 represent the system state variables, with $\hat{x}_1$ and $\hat{x}_2$ denoting their observed values. The parameters k_1 and k_2 correspond to sliding mode gain coefficients, while $\rho_1(\hat{x}_1,t)$ and $\rho_2(\hat{x}_1,t)$ characterize the system uncertainty terms.

By selecting the stator currents i_α and i_β as state variables and substituting $x_1=i_\alpha$ and $x_1=i_\beta$ into Equation (4), we establish the STA-SMO model as expressed in Equation (5):

$$\frac{d}{dt}\begin{bmatrix}\hat{i}_\alpha\\ \hat{i}_\beta\end{bmatrix}=-\frac{1}{L_d}\begin{bmatrix}k_1\left|\tilde{i}_\alpha\right|^{1/2}sgn(\tilde{i}_\alpha)+\int k_2 sgn(\tilde{i}_\alpha)\\ k_1\left|\tilde{i}_\beta\right|^{1/2}sgn(\tilde{i}_\beta)+\int k_2 sgn(\tilde{i}_\beta)\end{bmatrix}+\begin{bmatrix}\rho_1(\hat{i}_\alpha,t)\\ \rho_1(\hat{i}_\beta,t)\end{bmatrix} \tag{5}$$

where, $\hat{i}_\alpha$ and $\hat{i}_\beta$ represent the observed stator current values, with $\tilde{i}_\alpha$ and $\tilde{i}_\beta$ denoting the corresponding current observation errors. By subtracting Equation (3) from Equation (5), the stator current observation error dynamics can be derived as:

$$\frac{d}{dt}\begin{bmatrix}\tilde{i}_\alpha\\ \tilde{i}_\beta\end{bmatrix}=\frac{1}{L_d}\begin{bmatrix}-R_s & -\hat{\omega}_e(L_d-L_q)\\ \hat{\omega}_e(L_d-L_q) & -R_s\end{bmatrix}\begin{bmatrix}\tilde{i}_\alpha\\ \tilde{i}_\beta\end{bmatrix}+\frac{1}{L_d}\begin{bmatrix}\lambda_\alpha-v_\alpha\\ \lambda_\beta-v_\beta\end{bmatrix} \tag{6}$$

The stability conditions for the STA-SMO have been rigorously proven in [14]. When the observer achieves stability, the system states reach and maintain motion on the sliding surface. Under these conditions, the extended back-EMF can be derived from the equivalent control:

$$\begin{bmatrix}\lambda_\alpha\\ \lambda_\beta\end{bmatrix}_{eq}=\begin{bmatrix}v_\alpha\\ v_\beta\end{bmatrix}=\begin{bmatrix}k_1\left|\tilde{i}_\alpha\right|^{1/2}sgn(\tilde{i}_\alpha)+\int k_2 sgn(\tilde{i}_\alpha)dt\\ k_1\left|\tilde{i}_\beta\right|^{1/2}sgn(\tilde{i}_\beta)+\int k_2 sgn(\tilde{i}_\beta)dt\end{bmatrix} \tag{7}$$

4. Novel Fast Super-Twisting Sliding Mode Observer

4.1. Observer Design

To enhance both the dynamic response and steady-state estimation accuracy of the conventional STA-SMO, this paper proposes a FSTA, formulated as follows:

$$\begin{cases} u = -k_1[|x|^{1/2}\, sgn(x) + x] + u_1 \\ \dot{u}_1 = -k_2[\frac{1}{2} sgn(x) + \frac{3}{2}|x|^{1/2}\, sgn(x) + x] \end{cases} \tag{8}$$

Building upon the FSTA framework, we construct the FSTA-SMO as formulated in Equation :

$$\frac{d}{dt}\begin{bmatrix} \hat{i}_\alpha \\ \hat{i}_\beta \end{bmatrix} = -\frac{1}{L_d}\begin{bmatrix} k_1 g_1(\tilde{i}_\alpha) + \int k_2 g_2(\tilde{i}_\alpha) \\ k_1 g_1(\tilde{i}_\beta) + \int k_2 g_2(\tilde{i}_\beta) \end{bmatrix} + \begin{bmatrix} \rho(\hat{i}_\alpha, t) \\ \rho(\hat{i}_\beta, t) \end{bmatrix} \tag{9}$$

When the system enters sliding mode, the current error dynamics reduce to:

$$\frac{d}{dt}\begin{bmatrix} \tilde{i}_\alpha \\ \tilde{i}_\beta \end{bmatrix} = \frac{1}{L_d}\begin{bmatrix} -R_s & -\hat{\omega}_e(L_d - L_q) \\ \hat{\omega}_e(L_d - L_q) & -R_s \end{bmatrix}\begin{bmatrix} \tilde{i}_\alpha \\ \tilde{i}_\beta \end{bmatrix} + \frac{1}{L_d}\begin{bmatrix} \lambda_\alpha - v_\alpha \\ \lambda_\beta - v_\beta \end{bmatrix} \tag{10}$$

Under observer stability, the system states converge to the sliding surface. Applying the equivalent control principle, the reconstructed extended back-EMF via the FSTA-SMO yields:

$$\begin{bmatrix} \lambda_\alpha \\ \lambda_\beta \end{bmatrix}_{eq} = \begin{bmatrix} v_\alpha \\ v_\beta \end{bmatrix} = \begin{bmatrix} k_1 g_1(\tilde{i}_\alpha) + k_2 \int g_2(\tilde{i}_\alpha) \\ k_1 g_1(\tilde{i}_\beta) + k_2 \int g_2(\tilde{i}_\beta) \end{bmatrix} \tag{11}$$

This completes the estimation process of extended back-EMF through the FSTA-SMO framework, with the schematic structure illustrated in Fig. 1. To guarantee stability, rigorous Lyapunov-based analysis is conducted as follows:

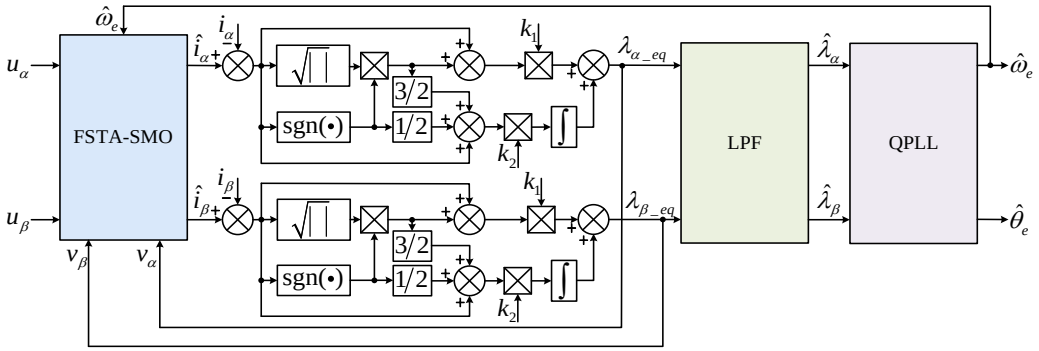

Figure 1: Schematic diagram of the FSTA-SMO structure.

4.2. Lyapunov Stability Analysis

To rigorously validate the stability of the proposed FSTA-SMO, we conduct a Lyapunov-based analysis using the current error dynamics in (12):

$$\begin{cases} \dot{\tilde{i}}_\alpha = -\sigma_1 g_1(\tilde{i}_\alpha) + \varphi(\tilde{i}_\alpha) + \rho_1(\tilde{i}_\alpha, t) \\ \dot{\varphi}(\tilde{i}_\alpha) = -\sigma_2 g_2(\tilde{i}_\alpha) + \rho_2(\tilde{i}_\alpha, t) \end{cases} \tag{12}$$

where, $\sigma_1 = k_1 / L_d$ and $\sigma_2 = k_2 / L_d$ are state variables.

Assume $\rho_1(\tilde{i}_\alpha, t)$ and $\rho_2(\tilde{i}_\alpha, t)$ satisfy the following boundedness condition:

$$\begin{cases} \rho_1(0,0) = 0 \\ \left|\rho_1(\tilde{i}_\alpha, t)\right| \le \delta_1 \left|g_1(\tilde{i}_\alpha)\right| \\ \left|\rho_2(\tilde{i}_\alpha, t)\right| \le \delta_2 \left|g_2(\tilde{i}_\alpha)\right| \end{cases} \tag{13}$$

where, δ_1 and δ_2 are positive constants. Let $\boldsymbol{\xi}^{\mathrm{T}} = \left[g_1(\tilde{i}_\alpha) \quad \varphi(\tilde{i}_\alpha) \right]$, from:

$$\begin{cases} g_1'(\tilde{i}_\alpha) = \dfrac{1}{2}\left|\tilde{i}_\alpha\right|^{-1/2} + 1 \ge 0 \\ g_2(\tilde{i}_\alpha) = g_1(\tilde{i}_\alpha) g_1'(\tilde{i}_\alpha) \end{cases} \tag{14}$$

We derive:

$$\dot{\boldsymbol{\xi}} = \begin{bmatrix} \dot{g}_1(\tilde{i}_\alpha) \\ \dot{\varphi}(\tilde{i}_\alpha) \end{bmatrix} = g_1'(\tilde{i}_\alpha) \left(\begin{bmatrix} -\sigma_1 & 1 \\ -\sigma_2 & 0 \end{bmatrix} \begin{bmatrix} g_1(\tilde{i}_\alpha) \\ \varphi(\tilde{i}_\alpha) \end{bmatrix} + \begin{bmatrix} \rho_1(\tilde{i}_\alpha, t) \\ \rho_2(\tilde{i}_\alpha, t) / g_1'(\tilde{i}_\alpha) \end{bmatrix} \right) = g_1'(\tilde{i}_\alpha) \left(\boldsymbol{A}\boldsymbol{\xi} + \boldsymbol{B} \right) \tag{15}$$

where, $\boldsymbol{A} = \begin{bmatrix} -k_1 & 1 \\ -k_2 & 0 \end{bmatrix}$ and $\boldsymbol{B} = \begin{bmatrix} B_1 \\ B_2 \end{bmatrix} = \begin{bmatrix} \rho_1(\tilde{i}_\alpha, t) \\ \rho_2(\tilde{i}_\alpha, t) / g_1'(\tilde{i}_\alpha) \end{bmatrix}$.

Based on the assumption in (13), we obtain:

$$\begin{cases} \left|B_1\right| = \left|\rho_1(\tilde{i}_\alpha, t)\right| \le \delta_1 \left|g_1(\tilde{i}_\alpha)\right| \\ \left|B_2\right| = \left|\rho_2(\tilde{i}_\alpha, t) / g_1'(\tilde{i}_\alpha)\right| \le \delta_2 \left|g_1(\tilde{i}_\alpha)\right| \end{cases} \tag{16}$$

An equivalent form of (16) can be expressed as:

$$H = c_1 \left(-B_1^2 + \delta_1^2 \left|g_1(\tilde{i}_\alpha)\right|^2 \right) + c_2 \left(-B_2^2 + \delta_2^2 \left|g_1(\tilde{i}_\alpha)\right|^2 \right) \ge 0 \tag{17}$$

where, c_1 , c_2 are positive constants. Equation (17) can be further rewritten as:

$$H = \begin{bmatrix} \boldsymbol{\xi} \\ \boldsymbol{B} \end{bmatrix}^{\mathrm{T}} \begin{bmatrix} (c_1\delta_1^2 + c_2\delta_2^2)\boldsymbol{D}^{\mathrm{T}}\boldsymbol{D} & \\ & -\boldsymbol{C} \end{bmatrix} \begin{bmatrix} \boldsymbol{\xi} \\ \boldsymbol{B} \end{bmatrix} \ge 0 \tag{18}$$

where, $\boldsymbol{D} = \begin{bmatrix} 1 & 0 \end{bmatrix}$, $\boldsymbol{C} = \begin{bmatrix} c_1 & \\ & c_2 \end{bmatrix}$.

Define the positive definite matrix $\boldsymbol{P}$ as:

$$\boldsymbol{P} = \begin{bmatrix} \dfrac{4a + b^2}{2} & \dfrac{-b}{2} \\ \dfrac{-b}{2} & 1 \end{bmatrix}, a > 0, b > 0 \tag{19}$$

Let:

$$\boldsymbol{A}^{\mathrm{T}}\boldsymbol{P}+\boldsymbol{P}\boldsymbol{A}+\varepsilon_1\boldsymbol{I}+(c_1\delta_1^2+c_2\delta_2^2)\boldsymbol{D}^{\mathrm{T}}\boldsymbol{D}+\boldsymbol{P}\boldsymbol{C}^{-1}\boldsymbol{P}=\boldsymbol{Q}=\begin{bmatrix}Q_{11} & Q_{12}\\ Q_{21} & Q_{22}\end{bmatrix} \tag{20}$$

where, ε_1 is a sufficiently small positive constant. After computation, we obtain:

$$\begin{cases} Q_{11}=-(4a+b^2)\sigma_1+b\sigma_2+\varepsilon_1+c_1\delta_1^2+c_2\delta_2^2+\dfrac{(4a+b^2)^2}{4c_1}+\dfrac{b^2}{4c_2} \\ Q_{12}=Q_{21}=\dfrac{b}{2}\sigma_1-\sigma_2+\dfrac{4a+b^2}{2}-\dfrac{b(4a+b^2)}{4c_1}-\dfrac{b}{2c_2} \\ Q_{22}=\varepsilon_1-b+\dfrac{b^2}{4c_1}+\dfrac{1}{c_2} \end{cases} \tag{21}$$

If the coefficients σ_1, σ_2, ε_1 satisfy:

$$\begin{cases} \sigma_1\geq\dfrac{2}{8a+b^2}\left[\varepsilon_1+c_1\delta_1^2+c_2\delta_2^2+\dfrac{b(4a+b^2)}{2}+\dfrac{a(4a+b^2)}{c_1}-\dfrac{b^2}{4c_2}\right] \\ \sigma_2=\dfrac{b}{2}\sigma_1+\dfrac{4a+b^2}{2}-\dfrac{b(4a+b^2)}{4c_1}-\dfrac{b}{2c_2} \\ \varepsilon_1\leq b-\dfrac{b^2}{4c_1}-\dfrac{1}{c_2} \end{cases} \tag{22}$$

then $Q_{11}<0$, $Q_{12}=Q_{21}=0$ and $Q_{22}<0$ is negative semidefinite. Let:

$$\boldsymbol{\Phi}=\begin{bmatrix}\boldsymbol{A}^{\mathrm{T}}\boldsymbol{P}+\boldsymbol{P}\boldsymbol{A}+\varepsilon_1\boldsymbol{I}+(c_1\delta_1^2+c_2\delta_2^2)\boldsymbol{D}^{\mathrm{T}}\boldsymbol{D} & \boldsymbol{P}\\ \boldsymbol{P} & -\boldsymbol{C}\end{bmatrix} \tag{23}$$

From the properties of block matrices, $\boldsymbol{\Phi}$ is negative semidefinite. Selecting a quadratic Lyapunov function candidate $V=\boldsymbol{\xi}^{\mathrm{T}}\boldsymbol{P}\boldsymbol{\xi}$, we have:

$$\begin{aligned}\dot{V}&=g_1'(\tilde{i}_\alpha)\left(\begin{bmatrix}\boldsymbol{\xi}\\ \boldsymbol{B}\end{bmatrix}^{\mathrm{T}}\begin{bmatrix}\boldsymbol{A}^{\mathrm{T}}\boldsymbol{P}+\boldsymbol{P}\boldsymbol{A} & \boldsymbol{P}\\ \boldsymbol{P} & \boldsymbol{0}\end{bmatrix}\begin{bmatrix}\boldsymbol{\xi}\\ \boldsymbol{B}\end{bmatrix}\right)\leq g_1'(\tilde{i}_\alpha)\left(\begin{bmatrix}\boldsymbol{\xi}\\ \boldsymbol{B}\end{bmatrix}^{\mathrm{T}}\begin{bmatrix}\boldsymbol{A}^{\mathrm{T}}\boldsymbol{P}+\boldsymbol{P}\boldsymbol{A} & \boldsymbol{P}\\ \boldsymbol{P} & \boldsymbol{0}\end{bmatrix}\begin{bmatrix}\boldsymbol{\xi}\\ \boldsymbol{B}\end{bmatrix}+H\right)\\ &\leq -g_1'(\tilde{i}_\alpha)\varepsilon_1\|\boldsymbol{\xi}\|_2^2\end{aligned} \tag{24}$$

Combining with the following inequality:

$$\lambda_{\min}(\boldsymbol{P})\|\boldsymbol{\xi}\|_2^2\leq\boldsymbol{\xi}^{\mathrm{T}}\boldsymbol{P}\boldsymbol{\xi}\leq\lambda_{\max}(\boldsymbol{P})\|\boldsymbol{\xi}\|_2^2 \tag{25}$$

We further derive:

$$\dot{V}\leq -g_1'(\tilde{i}_\alpha)\varepsilon_1\frac{V}{\lambda_{\max}(\boldsymbol{P})}=-\frac{1}{2}\bullet\frac{\varepsilon_1}{\lambda_{\max}(\boldsymbol{P})}\left|\tilde{i}_\alpha\right|^{-1/2}V-\frac{\varepsilon_1}{\lambda_{\max}(\boldsymbol{P})}V \tag{26}$$

Conclusion of Stability Proof: If there exist parameters δ_1, δ_2 such that $\rho_1(\hat{i}_\alpha,t)$, $\rho_2(\hat{i}_\alpha,t)$

satisfy the constraints in (13), and the sliding mode gains σ_1, σ_2 are selected according to (22), then $V \geq 0$ and $\dot{V} \leq 0$, thereby fulfilling the Lyapunov stability theorem.

4.3. Rotor Information Demodulation

To obtain smoothed estimates of the extended back-EMF signals, LPF is employed to attenuate high-frequency components. The filtered extended back-EMF can be mathematically expressed as:

$$\begin{bmatrix} \hat{\lambda}_\alpha \\ \hat{\lambda}_\beta \end{bmatrix} = \frac{\omega_c}{s+\omega_c} \begin{bmatrix} \lambda_{\alpha\_eq} \\ \lambda_{\beta\_eq} \end{bmatrix} \tag{27}$$

where, ω_c represents the cutoff frequency of the LPF. Due to the phase delay caused by the use of a LPF, phase compensation is required. Following back-EMF acquisition, a QPLL is employed to extract rotor position and speed information, with its structure illustrated in Fig. 2.

Under ideal conditions considering only the fundamental-frequency component of the extended back-EMF, the error correction term ε fed into the PI regulator satisfies:

$$\varepsilon = -\hat{\lambda}_\alpha \cos\hat{\theta}_e - \hat{\lambda}_\beta \sin\hat{\theta}_e = \lambda(\sin\theta_e \cos\hat{\theta}_e - \cos\theta_e \sin\hat{\theta}_e) = \lambda \sin(\theta_e - \hat{\theta}_e) \tag{28}$$

For small estimation errors ($\left|\theta_e - \hat{\theta}_e\right| < \pi/6$), the approximation $\sin(\theta_e - \hat{\theta}_e) \approx \theta_e - \hat{\theta}_e$ holds via the equivalent infinitesimal principle. Substituting into (28) yields the simplified error term:

$$\varepsilon = \lambda(\theta_e - \hat{\theta}_e) \approx \theta_e - \hat{\theta}_e \tag{29}$$

where, θ_e is the actual electrical angle and $\hat{\theta}_e$ the QPLL estimate.

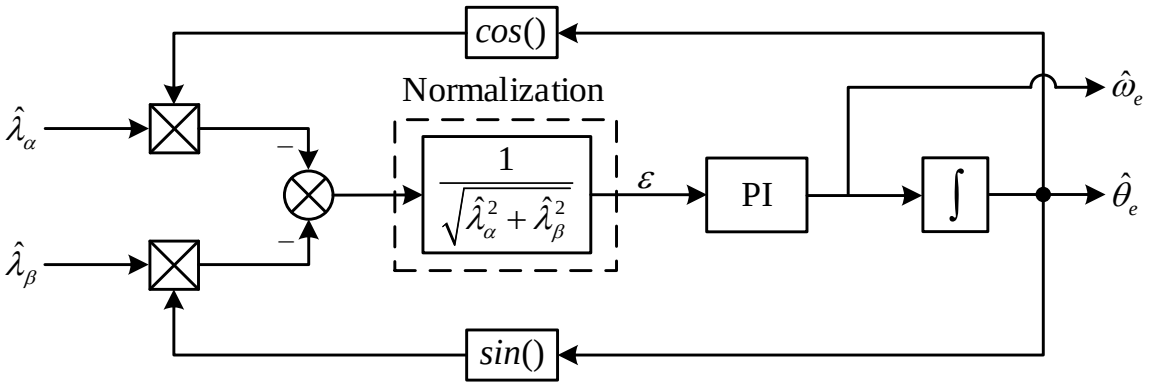

Figure 2: Schematic diagram of the QPLL structure.

5. Simulation

To verify the effectiveness and superiority of the proposed FSTA-SMO particularly its advantages in dynamic response and steady-state accuracy over the conventional STA-SMO we developed MATLAB/Simulink models of sensorless vector control systems for Interior Permanent Magnet Synchronous Motor (IPMSM) employing both observers for comparative analysis. The system structure with FSTA-SMO is illustrated in Fig. 3.

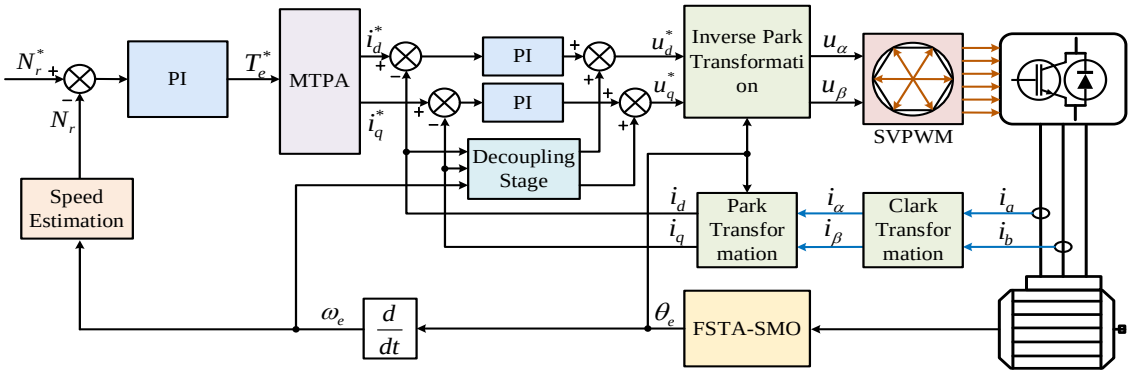

Figure 3: Schematic diagram of the Sensorless Vector Control System for IPMSM.

The simulation employs an IPMSM with parameters detailed in Table 1.

Table 1: IPMSM Simulation Experimental Parameters Table.

Parameter	Value/Unit
Number of Pole Pairs	4
d-axis Inductance	5.3mH
q-axis Inductance	12mH
Moment of Inertia	$0.003\,\mathrm{kg}\cdot\mathrm{m}^2$
Stator Resistance	$0.958\,\Omega$
Rotor PM Flux Linkage	0.1827 Wb

Under the condition of sudden load changes, the motor is set to start under no-load conditions with a target speed of 1500 r/min. The total simulation time is 0.6 seconds. A sudden load of 6 Nm is applied at 0.15 s and removed at 0.35 s, in order to observe the dynamic response characteristics of the two observation methods. Under sudden load variation, the speed waveforms of the two observation methods are shown in Fig. 4. As illustrated, the speed observed by the STA-SMO exhibits a noticeable delay and certain offset, along with relatively large speed fluctuations, which leads to increased observation error. In contrast, the speed waveform observed by the FSTA-SMO almost completely overlaps with the actual speed and shows a much smaller fluctuation amplitude.

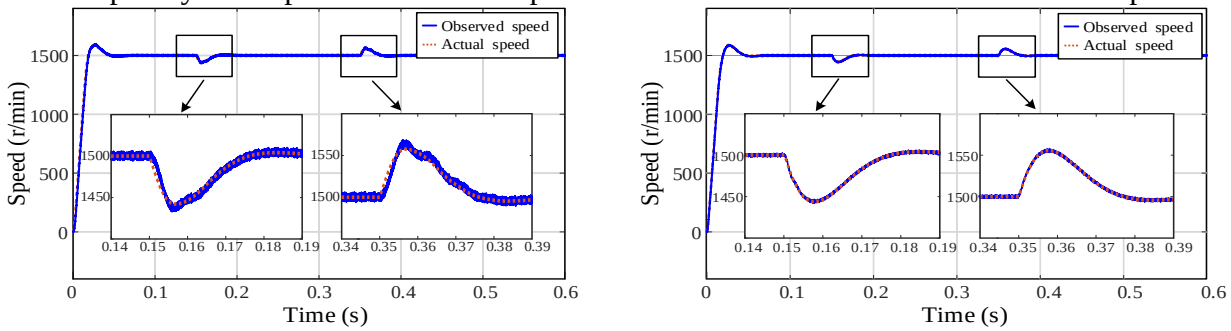

(a) STA-SMO (b) FSTA-SMO

Figure 4: Under Sudden Load Variation.

Figure 5 and 6 show the rotor position estimation errors of the two observation methods under sudden load changes. As seen in Fig. 5(a) and Fig. 6(a), when a sudden load is applied at 0.15 s, the STA-SMO exhibits a maximum rotor position error of 0.135 rad, accompanied by significant oscillations, with a final convergence time of approximately 0.028 s. In contrast, the FSTA-SMO shows an error of only 0.052 rad, with a smooth convergence process and no noticeable oscillations, requiring approximately 0.012 s to converge. Furthermore, from Fig. 5(b) and Fig. 6(b), it can be

observed that under the condition of sudden load removal, the STA-SMO has a maximum error variation of 0.132 rad, still accompanied by significant oscillations, and a convergence time of about 0.029 s. On the other hand, the FSTA-SMO exhibits a smaller error variation of only 0.049 rad, with no apparent oscillations, and the convergence time is reduced to 0.016 s.

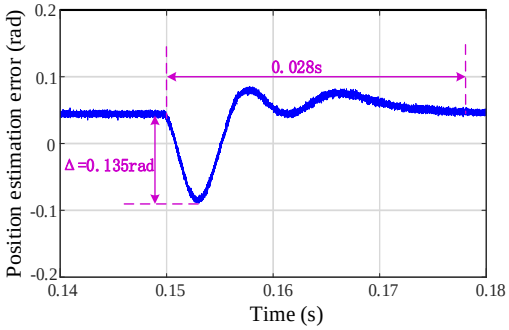

(c) STA-SMO

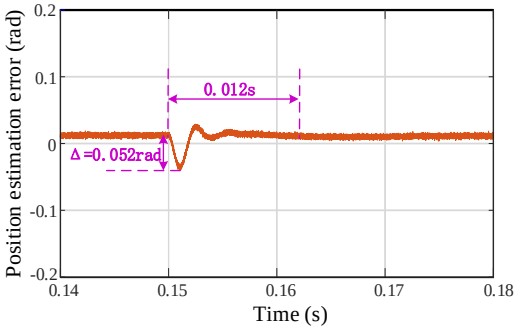

(d) FSTA-SMO

Figure 5: Under Sudden Load.

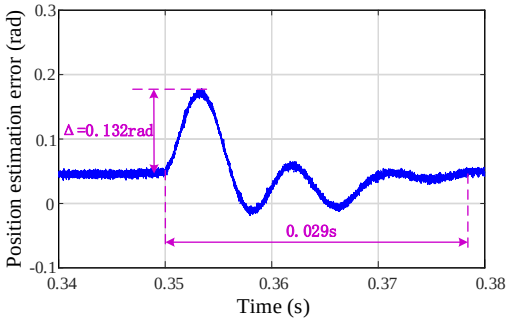

(a) STA-SMO

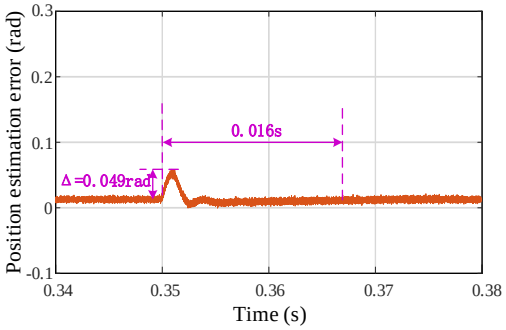

(b) FSTA-SMO

Figure 6: Under Sudden Load.

The above analysis indicates that under sudden load changes, the FSTA-SMO demonstrates faster response speed and higher estimation accuracy compared to the STA-SMO, showing superior observation performance.

6. Conclusions

This paper proposes a sensorless control method for PMSM based on FSTA-SMO. By introducing a linear term, the system achieves improved dynamic performance and steady-state accuracy. Simulation results demonstrate that FSTA-SMO offers higher estimation accuracy of rotor position and speed compared to STA-SMO, thereby enabling high-precision control of the PMSM.

References

[1] Anayi, & Fatih, J. . (2020). Estimation of rotor position for permanent magnet synchronous motor at standstill using sensorless voltage control scheme. IEEE/ASME Transactions on Mechatronics, 25(3), 1612-1621.

[2] Toso, F. , Berto, M. , Alberti, L. , & Marcuzzi, F. . (2019). Efficient qr updating factorization for sensorless synchronous motor drive based on high frequency voltage injection. IEEE Transactions on Industrial Electronics, PP(99), 1-1.

[3] Bui, M. X. , Guan, D. , Xiao, D. , & Rahman, M. F. . (2019). A modified sensorless control scheme for interior permanent magnet synchronous motor over zero to rated speed range using current derivative measurements. Industrial Electronics, IEEE Transactions on, 66(1), 102-113.

[4] Wang, G. , Xiao, D. , Zhao, N. , Zhang, X. , Wang, W. , & Xu, D. . (2017). Low-frequency pulse voltage injection scheme based sensorless control of ipmsm drives for audible noise reduction. IEEE Transactions on Industrial Electronics, PP(11), 1-1.
[5] Gaolin, Wang, Lei, Yang, & Guoqiang, et al. (2017). Comparative investigation of pseudorandom high-frequency signal injection schemes for sensorless ipmsm drives. IEEE Transactions on Power Electronics, 32(3), 2123-2132.
[6] Wang, B. , Huo, Z. , Yu, Y. , Luo, C. , Sun, W. , & Xu, D. . (2020). Stability and dynamic performance improvement of speed adaptive full-order observer for sensorless induction motor ultralow speed operation. IEEE Transactions on Power Electronics, 35(11), 12522-12532.
[7] Khlaief, A. , Boussak, M. , & Chaari, A. . (2014). A mras-based stator resistance and speed estimation for sensorless vector controlled ipmsm drive. Electric Power Systems Research, 108, 1-15.
[8] Kivanc, O. C. , & Ozturk, S. B. . (2018). Sensorless pmsm drive based on stator feedforward voltage estimation improved with mras multi-parameter estimation. IEEE/ASME Transactions on Mechatronics, 1-1.
[9] Quang, N. K. , Hieu, N. T. , & Ha, Q. P. . (2014). Fpga-based sensorless pmsm speed control using reduced-order extended kalman filters. IEEE Transactions on Industrial Electronics(61-12).
[10] Xuejian, C. , Bo, P. , Ling, L. , & Lin, G. . (2016). A novel nonsingular terminal sliding mode observer for sensorless control of permanent magnet synchronous motor. Journal of Xian Jiaotong University.
[11] Davila, J. , Fridman, L. , & Levant, A. . (2005). Second-order sliding-mode observer for mechanical systems. IEEE Transactions on Automatic Control, 50(11), 1785-1789.
[12] Gonzalez, T. , Moreno, J. A. , & Fridman, L. . (2012). Variable gain super-twisting sliding mode control. IEEE Transactions on Automatic Control, 57(8), 2100-2105.
[13] Evangelista, C. , Puleston, P. , Valenciaga, F. , & A. Dávila. (2010). Variable gains super-twisting control for wind energy conversion optimization. 2010 11th International Workshop on Variable Structure Systems (VSS). IEEE.
[14] Sreejith, R. , & Singh, B. . (2020). Sensorless predictive control of spmsm driven light ev drive using modified speed adaptive super twisting sliding mode observer with maf-pll. IEEE Journal of Emerging and Selected Topics in Industrial Electronics, PP(99), 1-1.